doi:10.1016/j.jmb.2007.01.051 J. Mol. Biol. (2007) 367, 1079–1092

JMB

Available online at www.sciencedirect.com

ScienceDirect

ELSEVIER

Propagation of Dynamic Changes in Barnase Upon Binding of Barstar: An NMR and Computational Study

Anastasia Zhuravleva[1,2], Dmitry M. Korzhnev[4], Svetlana B. Nolde[2] Lewis E. Kay[4], Alexander S. Arseniev[2], Martin Billeter[3] and Vladislav Yu. Orekhov[1]*

[1]*Swedish NMR Centre at Göteborg University, Box 465 405 30 Göteborg, Sweden*

[2]*Shemyakin-Ovchinnikov Institute of Bioorganic Chemistry, Russian Academy of Sciences, ul. Miklukho-Maklaya 16/10, Moscow, 117997, Russia*

[3]*Biophysics Group, Department of Chemistry, Göteborg University, Box 462 405 30 Göteborg, Sweden*

[4]*Departments of Medical Genetics, Biochemistry and Chemistry, University of Toronto, Toronto, Ontario Canada M5S 1A8*

**Corresponding author*

NMR spectroscopy and computer simulations were used to examine changes in chemical shifts and in dynamics of the ribonuclease barnase that result upon binding to its natural inhibitor barstar. Although the spatial structures of free and bound barnase are very similar, binding results in changes of the dynamics of both fast side-chains, as revealed by ^{2}H relaxation measurements, and NMR chemical shifts in an extended β-sheet that is located far from the binding interface. Both side-chain dynamics and chemical shifts are sensitive to variations in the ensemble populations of the inter-converting molecular states, which can escape direct structural observation. Molecular dynamics simulations of free barnase and barnase in complex with barstar, as well as a normal mode analysis of barnase using a Gaussian network model, reveal relatively rigid domains that are separated by the extended β-sheet mentioned above. The observed changes in NMR parameters upon ligation can thus be rationalized in terms of changes in inter-domain dynamics and in populations of exchanging states, without measurable structural changes. This provides an alternative model for the propagation of a molecular response to ligand binding across a protein that is based exclusively on changes in dynamics.

Keywords: deuterium relaxation; model-free; allostery; signal transduction

Introduction

Propagation of signals between distant sites in proteins contributes in a fundamental way to their role in living cells.[1] Examples include allosteric regulation of enzymes, signal transduction through membrane receptors and folding events. A common feature is that functionally important changes are observed at sites distant from the position of the initial perturbation caused, for example, by ligand binding, phosphorylation or a point mutation. For over 40 years, our understanding of long-range communication in proteins has evolved from the classical allosteric theory, which considers an induced switch between two states[2,3] to the landscape paradigm,[4–6] in which a protein under native conditions undergoes both small and large-scale thermal excursions to conformational states having similar energies. The resulting ensemble defines the native state.[7,8] Local perturbations, such as ligand binding, can lead to a net shift in the populations of conformers of the ensemble by coupling distant structural sites. These changes in populations may have little or no effect on the three-dimensional structure that can be observed by X-ray crystallography or NMR spectroscopy. Yet a transition to a functionally different state occurs, which does not necessarily replace the original ground state in the ensemble; instead, it may simply redistribute the populations of often sparsely populated but functionally important states.[9–11]

NMR spectroscopy provides a unique tool for studying various types of long-range communication in proteins. Apart from the detection of structural changes, the method allows the detailed characterization of the effects of binding or chemical

Abbreviations used: MD, molecular dynamics; RMSD, root-mean-square deviation; PCA, principal component analysis; GNM, Gaussian network model.

E-mail address of the corresponding author: orov@nmr.gu.se

modification on internal motions and on the populations in the ensemble of inter-converting states. The observed NMR chemical shifts and residual dipolar couplings are averages over the structural ensemble of the native state, and can be sensitive to even small changes in populations of this ensemble. Propagation of perturbations that do not affect the structure in a measurable way were recently observed experimentally in several protein systems as changes in side-chain dynamics,[12,13] residual dipole couplings,[14,15] and chemical shifts.[16]

For several decades, the barnase–barstar system has been thoroughly investigated by biophysical, biochemical and computational techniques. Notably, X-ray studies of barnase in the free and barstar-bound forms establish that there are very few differences in structure.[17] An extended network of thermodynamically linked residues was suggested for barnase on the basis of the results of computer simulations aimed at an exhaustive sampling of the effects of mutations on the distributions of conformational states.[18] For this small and overall "typical" globular protein, several hydrophobic cores[19] and dynamic domains[20,21] were proposed. In this work, we examine the effects of binding of the extracellular ribonuclease barnase (12.4 kDa) to its natural inhibitor barstar (10.2 kDa) using ^{1}HN, ^{15}N, $^{13}C^{\alpha}$, $^{13}C^{\beta}$ and methyl chemical shift perturbation analysis, and ^{2}H NMR relaxation measurements. Changes in these NMR parameters for 11 residues could not be explained by barstar binding or by the small structural differences between the free and bound forms. Supported by several computational approaches, a number of dynamic domains are characterized, and it is proposed that their relative motion provides an intrinsic mechanism for coupling between structurally distant sites in barnase. This type of dynamic coupling, which is not detected in experimentally determined structures, may represent an alternative mechanism for the propagation of signal between distant sites in proteins.

Results

In an effort to understand how binding with barstar affects the structural ensemble of extracellular ribonuclease barnase, we have combined detailed NMR analyses of binding-induced changes on both side-chain dynamics using ^{2}H relaxation measurements and on chemical shifts of ^{1}HN, ^{15}N, $^{13}C^{\alpha}$, $^{13}C^{\beta}$ and methyl ^{1}H, ^{13}C nuclei with molecular dynamics calculations and other computational approaches. We refrain from the analysis of backbone dynamics using ^{15}N NMR relaxation measurements, since the mobility of the backbone in the rather rigid dynamic domains (see below) is likely less affected by binding than side-chain motions, and because the analysis of ^{15}N relaxation data for the complex is not accurate enough due to transient dimerization involving barstar molecules (see Materials and Methods). Much of the analysis relies on high-resolution X-ray structures of free and bound barnase, which characterize the binding interface but show very little variation in the barnase structure apart from the immediate vicinity of the binding interface.

Changes in side-chain dynamics and chemical shifts in barnase upon binding with barstar

Side-chain dynamics of free barnase and its complex with barstar were studied by ^{2}H relaxation measurements performed on all 49 side-chain methyl groups. For each methyl group, four deuterium quadrupolar relaxation rates were measured at magnetic fields of 11.7 T, 14.1 T and 18.8 T; namely, the decay of longitudinal, $R^{Q}(D_z)$, transverse in-phase, $R^{Q}(D_+)$, transverse anti-phase, $R^{Q}(D_+D_z + D_zD_+)$, and quadrupolar order, $R^{Q}(3D_z^2\text{-}2)$.[22] The resulting ^{2}H relaxation rates were analyzed on a per residue basis using the model-free approach.[23,24] Specifically, the motion of each side-chain methyl group in barnase was described by: (i) an order parameter of picosecond time-scale motions S^2_{axis} quantifying mobility of the methyl rotation axis; (ii) a correlation time characterizing the time-scale of internal motions τ_e; and (iii) an effective overall rotation correlation time τ_R^{eff}, which includes contributions from both overall molecular tumbling and nanosecond time-scale internal motions.

Figure 1 summarizes the extracted model-free parameters for 41 and 38 of 49 methyl groups of free and barstar-bound barnase, respectively, that show good fits of ^{2}H relaxation data according to χ^2 statistics (using a 5% probability cut-off) and have uncertainties in S^2_{axis} and τ_e values below 20%. The order parameters S^2_{axis} and correlation times τ_e span ranges of 0.2–1 and 10–110 ps, respectively. This variation is in line with results reported for other proteins.[25,26] Both S^2_{axis} and τ_e were used to monitor the changes in methyl dynamics in barnase upon binding barstar. Statistically significant differences in either S^2_{axis} or τ_e (i.e. with a probability of 5% or less of obtaining the observed difference by chance according to Z-statistics) were found for five methyl groups shown in color in Figure 1 and listed in Table 1.

Chemical shift differences between free barnase and its barstar-bound form were measured for a total of 456 nuclei, including backbone ^{1}HN, ^{15}N, $^{13}C^{\alpha}$, $^{13}C^{\beta}$ and side-chain methyl ^{1}H, ^{13}C spins. For each nucleus type, the chemical shifts in free and in bound barnase were compared and standard deviations calculated; differences in chemical shifts on an individual basis were considered statistically significant if they exceeded two standard deviations. The 26 residues for which significant differences were observed are listed in Table 1.

Changes of both methyl dynamics and chemical shifts in barnase upon binding barstar are summarized in Table 1. Statistically significant differences, as defined above, in either side-chain dynamics or chemical shifts were observed for a total of 28 residues. These residues can be separated into three groups on the basis of their positions in the structure

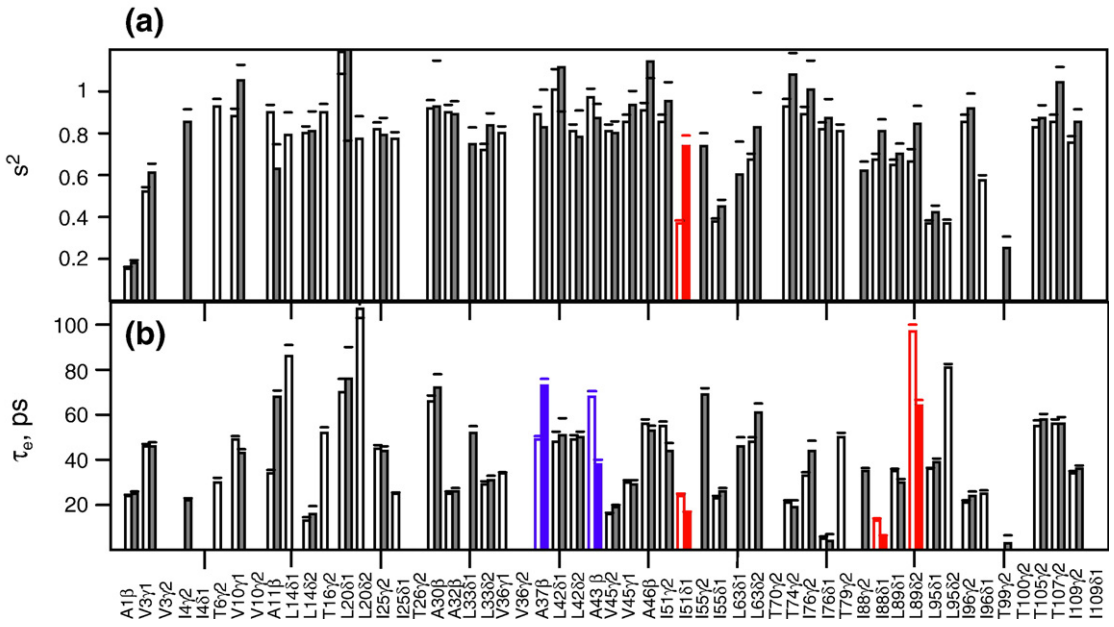

Figure 1. Parameters resulting from the model-free analysis: (a) The axial order parameters (S^2_{axis}) for free barnase (open bars) and the barnase–barstar complex (filled bars). (b) The correlation time of internal motions (τ_e) for free barnase (open bars) and the barnase–barstar complex (filled bars). Methyl groups showing statistically significant changes in corresponding dynamic parameters are highlighted in color: blue for those close to the barstar-binding interface or located in regions with significant differences in the X-ray structures of free and bound barnase; red for other methyl groups.

of barnase. The first group, denoted by B in the Position column of Table 1, consists of 14 residues adjacent to the binding interface, i.e. with atoms within 6.5 Å of any heavy atom of barstar. These residues are sufficiently close to barstar to be affected directly by changes in environment and local structure upon complex formation. The second group of three residues (S in Table 1) exhibits measurable atom displacements upon binding, i.e. differences in atom positions in free and complexed barnase exceed by a factor of at least 2 the variations observed for different structures of free and complexed barnase. The differences in dynamics or chemical shifts between free and bound barnase for these residues can be attributed to local conformational changes caused by complex formation. The remaining 11 residues (BR in Table 1), including three of the five methyl groups with significant changes in side-chain dynamics, are located far from the binding interface (>7.5 Å) and exhibit no significant structural change upon binding. The differences in side-chain dynamics and chemical shifts observed for these residues are due to long-range changes induced by barstar binding that cannot be explained on the basis of static three-dimensional structures. Indeed, differences in the order parameters predicted for these methyl groups from static X-ray structures, based on a method developed by Ming and Bruschweiler that calculates order parameters on the basis of local atom density and the number of dihedral angles between the methyl group and the protein backbone,[27] were an order of magnitude smaller than those measured in this work.

Molecular dynamics (MD) simulations of free and barstar-bound barnase

MD simulations can provide additional clues to understanding how binding might induce long-range effects in side-chain dynamics and in NMR chemical shifts. To this end, a pair of 30 ns MD simulations were generated, one for free barnase and one for the barnase–barstar complex. Figure 2 shows root-mean-square deviations (RMSDs) between all barnase structure pairs for each of the two MD traces, illustrating that both trajectories were stable. Note that somewhat lower RMSD values were observed in the MD trajectory of the complex as compared to that for free barnase (average RMSD of 0.8 Å and 1.3 Å, respectively).

Calculation of order parameters S^2_{axis} for side-chain methyl groups of barnase from the MD trajectories can be used to establish the consistency between MD simulations and NMR experiments. The correlation coefficients for the methyl order parameters between the experiment and the MD simulations are about 0.55 for both free and complexed barnase, in line with similar comparisons reported for other globular proteins.[28] A detailed comparison between experiment and MD is beyond the scope of the present work, especially considering the limited success of MD to predict these order parameters in general.

The main goal of the MD simulations is to correlate the differences in collective dynamics of free and barstar-bound barnase observed in the simulations with changes in experimental parameters. To reveal concerted motions in the MD runs of free barnase

Table 1. Residues in barnase exhibiting significant changes in chemical shifts and/or methyl dynamics upon binding with barstar

Residue	CS $p(\chi^2)$[a] (%)	Dyn $p(\chi^2)$[a] (%)	Distance[b] (Å)	Position[c]	Atom name[d]	Secondary structure[e]
59	0.14		3.2	B	C^{β}	
37	<0.1	<0.1	3.7	B	C^{β}	
85	<0.1		4.2	B	H, N, C^{α}	
60	<0.1		4.3	B	C^{α}	
84	<0.1		4.4	B	N	
104	<0.1		4.5	B	C^{β}	
82	0.7		4.7	B	C^{α}	
103	<0.1		4.9	B	H	
83	0.3		5.0	B	H	
102	<0.1		5.0	B	H, C^{β}	
27	<0.1		5.0	B	H, N, C^{α}, C^{β}	α2
58	<0.1		5.3	B	C^{β}	
86	<0.1		6.4	B	H	
101	3.6		6.5	B	N	
36	0.9		8.5	S	H, C^{β}	
41	<0.1		8.5	S	H	
43	16.5	<0.1	13.7	S		α3
24	2.9		13.2	BR(1)	C^{β}	β1
25	3.3	68.9	12.6	BR(1)	N	β1
51	<0.1	0.1	7.6	BR(2)	C^{α}, C^{β}, $C^{\delta 1}$	β2
52	3.9		9.4	BR(2)	C^{α}	β2
54	0.2		7.7	BR(2)	H, C^{α}, N	β2
71	3.5		8.8	BR(3)	C^{β}	β3
72	3.9		9.7	BR(3)	C^{α}	β3
73	2.9		7.6	BR(3)	C^{β}	β3
88	7.5	0.2	11.9	BR(4)		β4
89	0.1	0.4	10.7	BR(4)	N, C^{α}	β4
90	2.8		13.1	BR(4)	C^{α}	β4

[a] Values of $p(\chi^2)$ <5% indicate that the change in chemical shifts (CS) or in model-free parameters describing side-chain methyl dynamics (Dyn) is statistically significant. Only the residues exhibiting at least one statistically significant change with $p(\chi^2)$ <5% are listed.

[b] Distance between the atom in barnase showing significant changes in NMR parameters and the nearest heavy-atom in barstar (if several atoms in the residue exhibit significant changes, the one with the lowest value of $p(\chi^2)$ is chosen).

[c] Grouping of residues: Changes that can be explained by proximity to the barstar-binding interface or by noticeable changes in the structure of barnase upon binding, are indicated by B or S, respectively. Residues belonging to one of the bending regions between the dynamic domains obtained in MD simulations and normal mode analysis (Figure 3) are identified by BR(*n*), where *n* is the number of the bending region.

[d] Atom(s) showing statistically significant changes in chemical shifts.

[e] Secondary structure identifications are given in the legend to Figure 3.

and of the barnase–barstar complex, we have performed a principal component analysis (PCA).[29] The approach decomposes the complex picture of atomic motions in the protein molecule that are observed in MD simulations into a set of independent principal modes. Each of the two MD traces was divided into ten 3 ns segments that were used independently as input for PCA. The fluctuations along the resulting highest-amplitude modes can be represented as motions of dynamic domains. Therefore, the three first PCA modes from each segment were analyzed using the approach described by Hayward and co-workers with the goal of finding a minimal set of relatively rigid so-called dynamic domains, separated by bending regions.[30,31] Figure 3 shows five stretches of residues in the amino acid sequence of barnase, denoted M1 to M5, which move as relatively rigid modules (residues 6–23, 25–51, 54–74, 75–87, and 90–107, respectively). These modules were consistently revealed in analyses of modes in all of the MD segments for free and bound barnase (total $10 \times 3 \times 2$ PCA modes; see Materials and Methods for details). In the three-dimensional structure, these modules can be grouped into a smaller number of relatively rigid dynamic domains. The picture of dynamic domains varies somewhat between different modes and MD segments. The modules M1 and M2 are always associated with two different domains. In some cases, modules M3 to M5 form a single dynamic domain together with M1. In alternative situations, module M4 joins M2 in forming the second domain, while the first domain consists of modules M1, M3 and M5. Residues in the bending regions allow for motions of the dynamic domains.

Other computational approaches

Collective motions over a wide range of timescales extending beyond the limits accessible for MD simulations were characterized using an extension of the Gaussian Network Model (GNM).[32,33] In GNM, an elastic network is built on the basis of inter-residue contact topology using positions of C^{α} atoms from a PDB structure as input. Subsequently, collective motions in the network are analyzed by normal mode analysis. The location of the bending regions defined by GNM using the barnase structures (Figure 3) is in agreement with the borders between the modules M1–M5 obtained from MD. Similar modules for barnase were obtained in pre-

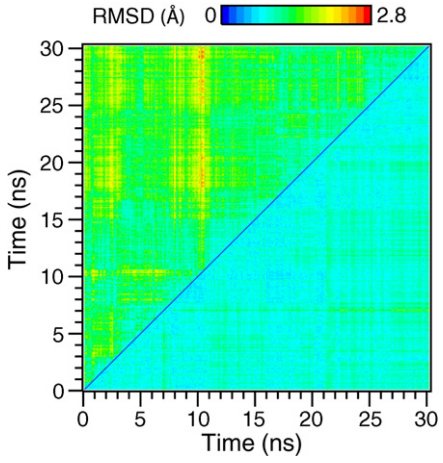

Figure 2. Pair-wise root-mean-square deviation (RMSD) for 300 structures taken on each 100 ps of the 30 ns MD trajectories for free barnase (upper triangle) and the complex (lower triangle). The RMSDs for barnase structures are calculated using N, C′, C^{α}, and C^{β} atoms for residues 5–110.

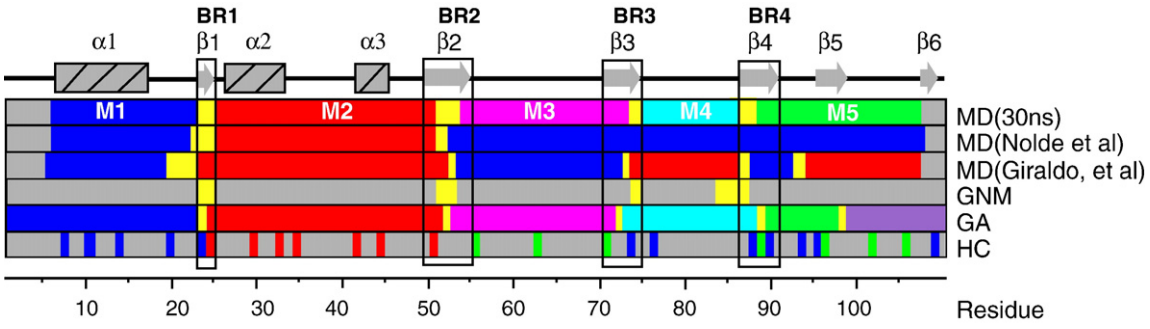

Figure 3. Localization of rigid modules and bending regions (shown in yellow) in barnase as defined by different computational methods. *MD(30ns),* results of analysis of 30 ns traces for free and barstar-bound barnase; five rigid modules, M1–M5, are shown in different colors. *MD(Nolde et al.)* and *MD(Giraldo et al.),* two dynamic domains are shown as reported in previous MD studies of free barnase;[20,21] the domains (blue and red) may consist of one or several modules. *GNM,* definition of the bending regions from the GNM analysis. *GA,* six modules as defined in a published geometric analysis of the barnase crystal structure;[34] the modules are shown in different colors. *HC,* residues forming three hydrophobic cores in barnase:[19] HC1(blue), HC2(red) and HC3(green). At the top of the Figure, elements of secondary structure in barnase are identified. The annotated rectangles BR1–BR4 (β-strands β1–β4; residues 24–25, 50–55, 71–75, and 87–91, respectively) indicate the bending regions assumed in this work. Regions uncharacterized by a given method are shown in gray.

vious studies of free barnase using geometrical analysis[34] and shorter MD simulations (Figure 3).[20,21]

Inter-domain motions and bending regions

The results of the MD simulations and the normal mode analysis presented here, along with those reported in previous work, demonstrate consistently that collective motions in barnase can be represented by changes in the populations of various states adopted by the five modules M1–M5, which in turn may be grouped into several relatively rigid dynamic domains. The modules are connected by four short bending regions. While their position varies slightly, depending on the different methods of calculation (Figure 3), these bending regions are always part of the four short β-strands β1–β4, which form an extended β-sheet in barnase.

A major result of the present study is that this extended β-sheet, which is located far from the binding site, also contains the 11 residues with significant binding-induced changes in NMR chemical shifts and side-chain dynamics that cannot be explained by proximity to the binding interface or by differences in spatial structures of free and barstar-bound barnase (Table 1). In the complex, barstar interacts with modules M2 and M3–M5 of barnase, which belong to different dynamic domains. The binding event can then be propagated to distal sites in the protein through the bending regions, mentioned above. As we describe below, this can lead to changes in relative populations of the ensemble that, in turn, result in the observed changes in NMR parameters between apo and ligated protein, without affecting the observable three-dimensional structures.

Discussion

Significant changes in side-chain dynamics parameters and/or chemical shifts that accompany barstar binding are listed in Table 1 and illustrated by Figure 4. Changes for about two-thirds of the residues can be attributed to the proximity to barstar or to structural differences that are apparent from the crystallography (Figure 4(a)).[17] However, changes for the remaining 11 residues cannot be understood on the basis of the static picture provided by the experimentally determined three-dimensional structures of the free and bound states of barnase. Remarkably, all of these residues are located in the bending regions, which form an extended interface between the dynamic domains (Figure 4(b)). It is of interest that the pattern of dynamic domains in barnase corresponds roughly to the localization of three independent hydrophobic cores, HC1, HC2 and HC3, described previously (Figure 3).[19,35] For example, hydrophobic core HC1 is formed by residues from M1, M3, and M5; HC2 comprises residues of M2; and HC3 is formed by residues of M3 and M5. In what follows, we discuss how both chemical shifts and methyl ^{2}H relaxation of residues distant from the binding site can be sensitive reporters of binding, what the underlying reasons for changes in these parameters might be, and why such changes are restricted to the linker regions between the dynamic domains. Finally, the arrangement of the bending regions between the dynamic domains in barnase can be compared to networks of coupled residues described for other proteins,[1,36] allowing one to speculate on the possible roles of motion in dynamic domains in such networks as well.

Explanation of changes in experimental parameters

Chemical shifts observed in NMR spectra are population-weighted averages over all members of a structural ensemble (provided that the rates of interconversions are faster than the frequency differences between the states). Model-free order parameters

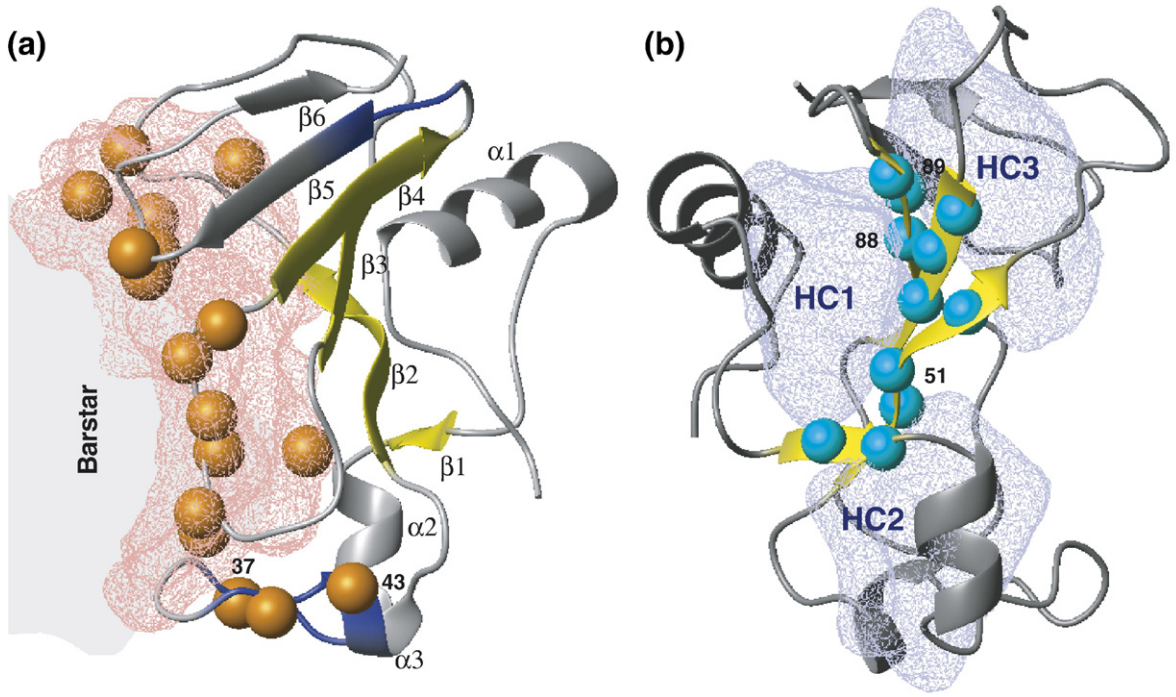

Figure 4. Mapping of changes in the NMR experimental parameters on the barnase structure (see Table 1). Spheres depict residues with significant differences. Those corresponding to altered methyl dynamics are annotated. The bending regions (defined in Figure 3) are shown in yellow. (a) Orange spheres indicate changes that can be explained by "structural factors". The red transparent surface shows barnase residues within 6.5 Å from any heavy atom of barstar. Regions distant from barstar but showing significant differences in the X-ray structures of free and bound barnase are highlighted in dark blue. (b) Residues for which changes cannot be explained by structural factors are shown as blue spheres. All these residues are located in β-strands β1–β4, which form the interface between the dynamic domains of barnase obtained in MD simulations and normal mode analysis. The three hydrophobic cores in barnase are depicted by transparent blue surfaces and annotated as HC1, HC2 and HC3. The structure is rotated clockwise relative to that shown in (a) by 140° if viewed from the top.

and correlation times of methyl groups, on the other hand, reflect amplitudes and rates of conformational transitions in the sub-nanosecond time-scale; motions with characteristic times longer than a few nanoseconds are effectively filtered out by overall molecular rotation and are not observed directly in the relaxation analysis. However, changes in motions on slower time-scales (but still in the fast exchange limit) can lead to changes in the pattern of the model-free relaxation parameters, since S^2_{axis} and τ_e values are ensemble averages, in a manner similar to chemical shifts and residual dipolar couplings. The sensitivity of these parameters to binding-induced changes in populations of the conformers of the ensemble depends on the distributions of their values among members within the ensemble. Notably, a number of computational studies indicate that, similar to chemical shifts, methyl dynamics can be sensitive to local spatial structure, that most certainly varies among interconverting conformers.[25,27,28,37] MD simulations of free barnase and the barnase–barstar complex have established that collective motion does occur on nanosecond time-scales and beyond, where the relaxation parameters are averaged similarly to chemical shifts. In the complex, barstar interacts with different dynamic domains in barnase, affecting collective motions.[17] Apart from the binding interface, the largest variation in local environment is expected where the domains contact each other, i.e. in the inter-domain interfaces. Therefore, it is not surprising that changes in NMR parameters are observed in the contact interfaces between the relatively rigid dynamic domains rather than within the domains. Moreover, the observed changes in model-free parameters can be explained by a re-distribution of the population of conformers within the ensemble, where the conformers have different side-chain mobilities, rather than differences in fast picosecond time-scale side-chain dynamics between free and bound states of barnase.

Relations between dynamic domains, stability and activity of barnase

Collective motions have been shown to have an important role in the long-range propagation of conformational changes across proteins.[9,38] In barnase, collective motions were correlated to stability and function, and it is interesting to try to extend this correlation to changes in experimental NMR parameters observed here. A number of mutational studies have demonstrated that residues located in the bending regions play essential roles for stability of barnase.[19,39,40] For example, substitutions of Gly52 and Gly53 with alanine were the most destabilizing for the protein, while the muta-

tion Ile51Val produces the largest destabilization among conservative substitutions of isoleucine or leucine with valine.[19] Hilser *et al*. showed with computer simulations of the equilibrium ensemble of protein conformations that residues 87–91 (bending region BR4, Figure 3) form a key energetic link in barnase.[18] Moreover, binding with GpAp that bridges the same residues in barnase as barstar influences significantly the collective motions that foster interactions with key catalytic residues.[21]

Relation to previous NMR results

There are a number of examples where long-range effects observed by NMR could not be explained on the basis of static structures. For example, binding of a target peptide to the PDZ domain from human tyrosine phosphatase 1E led to changes of methyl mobility in regions distant from the binding site without significant perturbation of the three-dimensional structure.[12] Methyl dynamics in the pico–nanosecond time-scale were perturbed at positions far from single-residue mutations in the B1 domain of protein L.[13] Similarly for the nucleotide binding domain (NBD) of the heat shock cognate chaperone protein (Hsc70), 14 different X-ray structures, which superimpose to within experimental error, could not explain changes of chemical shifts at remote sites upon binding with different ligands,[15] nor are they consistent with residual dipolar couplings measured in solution.

While the sensitivity of methyl dynamics to local structure is documented in a number of cases, the mechanism by which dynamic coupling between distant sites occurs in proteins remains unclear. A mechanistic model describing the dispersion of side-chain dynamics within a protein was suggested in an early methyl relaxation study.[26] In the model, which found support also in later studies, perturbations propagate through a network of adjacent side-chains having close van der Waals contacts. Clarkson & Lee reported that residues with side-chain dynamics affected by point mutations in the serine protease inhibitor eglin C form a contiguous surface or scattered in the protein structure up to 1.6 nm away from the position of mutation.[41,42] In the PDZ domain from human tyrosine phosphatase 1E, residues exhibiting significant changes in side-chain dynamics upon protein binding to a target peptide form two contiguous surfaces that can be linked to the binding site *via* short chains of van der Waals contacts.[12]

Collective motions and thermodynamic coupling networks in proteins

The direct link between collective motions and long-range propagation of binding-induced changes in barnase established in this work provides insight into the mechanism by which distant sites in proteins are coupled. Networks of energetic coupling are an essential property of protein structures, and are related to allostery and protein stability.[1] The networks have several common features including:[36] (i) only a relatively small fraction of the protein residues is involved; (ii) residues are often arranged in contiguous surfaces or clusters and appear as chains of van der Waals contacts; (iii) signal propagation through the network may or may not be accompanied by noticeable changes in protein structure; and (iv) the coupling may be asymmetric, so that a perturbation at one site propagates to the other but not necessarily back. These observations are descriptive; the present study provides some indication, at least in the context of the barnase–barstar system, as to why certain residues are selected to contribute to the transduction of perturbations, while the rest of the protein is not involved.

Groups of residues exhibiting long-range changes in side-chain dynamics and/or chemical shifts, such as those found here for barnase or previously for the PDZ domain, often overlap with those that form thermodynamically coupled networks within proteins.[18,36,43] Similar contiguous networks of thermodynamically coupled residues were identified using multiple gene sequence alignments for the serine protease and hemoglobin families as well as in the G-protein-coupled receptors.[44] In the latter case, the network of inter-helical van der Waals contacts links the ligand-binding pocket with the G-protein-interaction site.

Conclusions

We have shown that changes in methyl ^{2}H NMR relaxation parameters and in ^{1}H, ^{15}N and ^{13}C chemical shifts provide very sensitive measures of subtle binding-induced changes in the conformational ensemble of barnase, which remain undetected in the static pictures of the protein in its free and barstar-bound forms. Thus, with the use of NMR spectroscopy, we have characterized long-range changes in four β-strands of an extended β-sheet in barnase, which is remote from the binding site. These bending regions naturally form a network coupled through hydrogen bonds and arranged as a surface. This surface provides a mobile interface between relatively rigid dynamic domains, as revealed by MD simulations and normal mode analysis, that can "react" in a very sensitive manner to the ligand-binding event. It is tempting, therefore, to speculate that interfaces between rigid modules of proteins provide pathways for communication between distant sites, and that variations of ensemble populations may be a general mechanism for propagation of signals throughout the protein structure.

Materials and Methods

NMR sample preparation

Uniformly (^{15}N, ^{13}C)-enriched, 40% fractionally deuterated barnase was prepared as described.[45] A barnase–barstar complex was generated by adding aliquots from a

12 mM solution of purified barstar to a 1.3 mM barnase solution until monomer signals disappeared in ^{1}H-^{15}N 2D heteronuclear single quantum coherence spectra, which resulted in a final barnase to barstar molar ratio of 1:1 and a final complex concentration of 1.17 mM (based on amount of barstar added). A fraction of this sample was diluted to produce another sample of the barnase–barstar complex with a concentration of 0.17 mM. All experiments we performed in 10 mM potassium phosphate buffer at pH 6.5 ($H_2O/^2H_2O$, 9:1 (v/v)).

Chemical shift assignment of barnase in the complex; comparison with free barnase

Assignments for free barnase have been reported (BioMagResBank deposition code 4964);[45] assignments for the complex were obtained by transferring those from free barnase. A number of ambiguities and differences in signal positions between apo and ligated barnase were resolved using HNCACB, CBCA(CO)NH, (H)CC(CO) total correlated spectroscopy and H(CC)(CO)NH- total correlated spectroscopy spectra recorded on a Varian Inova 500 MHz spectrometer using standard BioPack (Varian Inc.) pulse sequences. Spectra were processed and analyzed using XEASY software.[46]

Differences in peak positions in the spectra of free and barstar-bound barnase were calculated for H^N, N, C^α, C^β atoms. In addition, combined chemical shift differences, $\Delta\delta(CH_{met})$, were calculated for methyl groups as:

$$\Delta\delta(CH_{met}) = [(\Delta\delta C^{ppm}_{met}/4)^2 + (\Delta\delta H^{ppm}_{met})^2]^{1/2} \qquad (1)$$

where $\Delta\delta H^{ppm}_{met}$ and $\Delta\delta C^{ppm}_{met}$ are chemical shift differences (measured in ppm) for methyl protons and carbon atoms, respectively. Chemical shifts for each nucleus type were compared between free and bound barnase, and the differences in shifts were considered significant if they exceeded twice the standard deviation calculated between data sets.

NMR relaxation experiments

All relaxation experiments were performed at 30 °C on Varian Inova spectrometers using an interleaved scheme for data acquisition and temperature control procedures described elsewhere.[47] The spectra were processed and quantified using NMRPipe,[48] MUNIN,[49] and DASHA[50] software packages as described.[51]

^{15}N relaxation measurements

^{15}N longitudinal (R_1) and transverse (R_2) relaxation rates were measured for free barnase and the barnase–barstar complex at 500 MHz (spectrometer ^{1}H Larmor frequency) using pulse sequences described previously.[52] Additionally, R_1 and R_2 experiments (600 MHz) were performed for a dilute barnase–barstar complex (0.17 mM concentration). Uncertainties in R_1 and R_2 were estimated as described,[47] with the lowest error set to 2%.

^{2}H relaxation measurements

^{2}H spin relaxation experiments for the quantification of side-chain methyl groups were performed by recording a series of ^{13}C-^{1}H correlation maps using pulse sequences described previously.[22] Four relaxation rates were measured for both free barnase and the barnase–barstar complex at 500 MHz, 600 MHz and 800 MHz, including $R^Q(D_z)$ (longitudinal magnetization), $R^Q(D_+)$ (transverse in-phase magnetization), $R^Q(3D_z^2\text{-}2)$ (quadrupolar order), and $R^Q(D_+D_z + D_zD_+)$ (transverse antiphase magnetization). Uncertainties in the deuterium relaxation rates were estimated as described,[47] with the lowest boundary set to 3%. Out of a total of 55 methyl groups, correlations from two pairs (V3γ2 and V36γ2, I4δ1 and I109δ1) were overlapped in ^{1}H-^{13}C correlation spectra of both apo and ligated barnase, and peaks derived from Ile88γ2 and T100γ2 are overlapped for free barnase, and rates were measured for the remaining 49 methyl groups.

Consistency of ^{2}H relaxation data

Up to five independent relaxation rates can be measured for a spin $I=1$ nucleus, such as a deuteron.[22] These rates are defined by values of the spectral density function at only three frequencies, 0, ω_D, and $2\omega_D$, where ω_D is the deuterium Larmor frequency. Thus, it is possible to verify the consistency of individual measurements before any analysis, which typically requires a number of assumptions for extraction of the dynamics parameters.[22] In particular, the following inequalities must hold:

$$\begin{aligned} 5/3R^Q(D_+D_Z + D_ZD_+) &\geq R^Q(D_+) \\ &\geq 5/3R^Q(3D_Z^2 - 2) \geq R^Q(D_Z) \end{aligned} \qquad (2)$$

Figure 5 shows the experimental relaxation rates measured at 500 MHz that have been multiplied by the prefactors indicated in equation (2) and the predicted set of inequalities are found to hold for data measured on both free and bound barnase. An additional relation that must hold if the data are consistent is (equation 13 of Millet *et al.*[22]):

$$R^Q(D_+D_Z + D_ZD_+) = R^Q(D_+) - 2/3\ R^Q(3D_Z^2 - 2) \quad (3a)$$

and Figure 6 shows that the experimentally derived rates $R^Q(D_+D_Z+D_ZD_+)$, $R^Q(D_+) - 2/3\ R^Q(3D_Z^2-2)$ follow this expected correlation very well. To quantify the correlation further, the following χ^2 value was calculated:

$$\chi^2 = \sum_i \frac{(R^Q_{i,L} - R^Q_{i,R})^2}{(\Delta R^Q_{i,L})^2 + (\Delta R^Q_{i,R})^2} \qquad (3b),$$

where $R^Q_{i,L}(\Delta R^Q_{i,L})$ and $R^Q_{i,R}(\Delta R^Q_{i,R})$ are linear combinations of experimental relaxation rates (estimated errors), given by the left-hand and right-hand sides of equation (3a), and the index i corresponds to different methyl groups. A data set was assumed to be self-consistent if $p(\chi^2) > 5\%$ (49 degrees of freedom = number of considered methyl groups). All of the six data sets (three magnetic fields, samples of either apo or ligated barnase) were consistent with equation (3a).

Model-free analysis [23,24] of ^{2}H relaxation rates

Dynamics parameters were extracted using DASHA software (version 4.1),[50] which was adapted for the analysis of methyl relaxation data. Parameters of side-chain methyl dynamics (S^2_{axis}, τ_e, τ_R^{eff}) were derived on a per-residue basis from minimization of the loss function of the form:

$$F(\zeta) = \sum_{i=1}^{N} \frac{(\Gamma_i^{th}(\zeta) - \Gamma_i^{exp})^2}{(\Delta\Gamma_i^{exp})^2} \qquad (4)$$

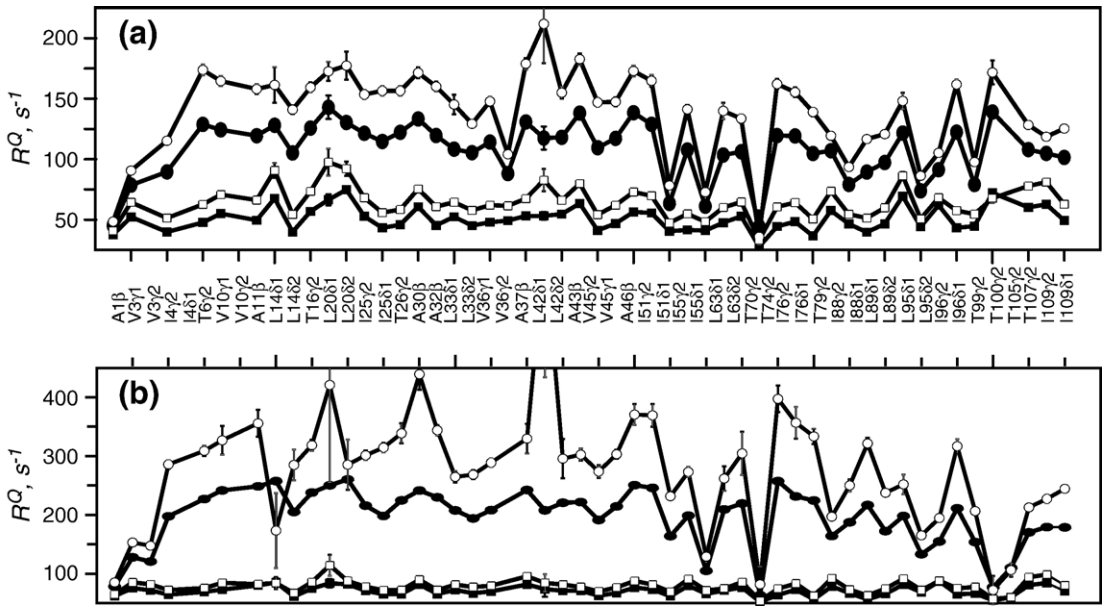

Figure 5. Plot of four experimental ^{2}H relaxation rates (500 MHz) as a function of residue (a) free barnase and (b) barnase in the complex. The rates, $5/3R^Q(D_+D_Z+D_ZD_+)$, $R^Q(D_+)$, $5/3R^Q(3D_Z^2-2)$, and $R^Q(D_Z)$ are shown as open circles, filled circles, open squares and filled squares, respectively.

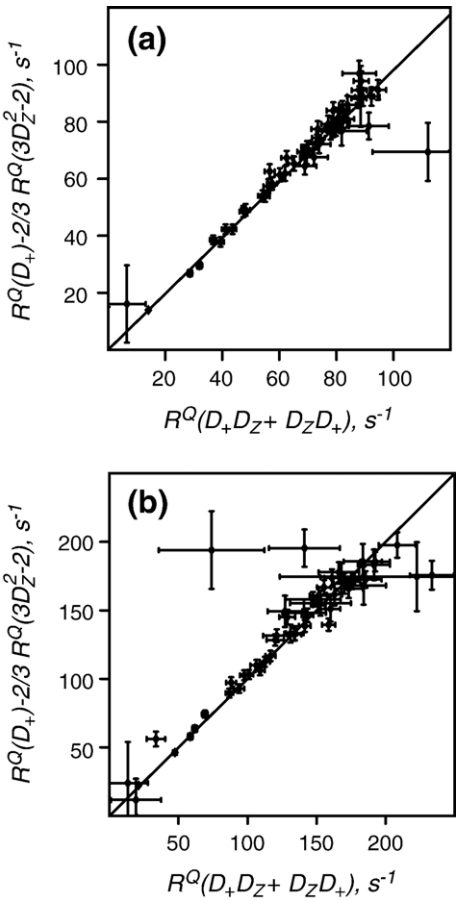

Figure 6. Consistency relations $R^Q(D_+)-2/3R^Q(3D_Z^2-2)$ *versus* $R^Q(D_+D_Z+D_ZD_+)$ for the experimental ^{2}H relaxation rates at 500 MHz: (a) free barnase; and (b) the barnase–barstar complex.

where Γ_i^{th} and $\Gamma_i^{\exp}$ are the calculated and experimental relaxation rates, respectively, and the index i distinguishes each of the 12 independent relaxation rates measured for each protein sample (three fields, four rates), and $\Delta\Gamma_i^{\exp}$ is the estimated error in the experimental relaxation rate i. We have used expressions for $\Gamma_i^{th}(\zeta)$ given in equation (1) of Skrynnikov *et al.*,[53] along with a deuterium quadrupole constant (e^2Qq/h) of 167 kHz and a spectra density function defined as:

$$J(\omega) = \frac{1}{9}S_{axis}^2\frac{\tau_R^{eff}}{1+\omega^2(\tau_R^{eff})^2} + \left(1-\frac{1}{9}S_{axis}^2\right)\frac{\tau}{1+\omega^2\tau^2} \quad (5)$$

$$1/\tau = (1/\tau_R^{\text{eff}}) + (1/\tau_e)$$

where τ_R^{eff} is the effective correlation time for overall molecular tumbling, τ_e is a correlation time for internal motions that includes both rotation about and of the methyl 3-fold axis and S^2_{axis} is an order parameter describing the amplitude of motion of the methyl axis. The factor 1/9 in equation (5) takes into account methyl rotation about its axis of symmetry. Fits are successful if $p(\chi^2)$ >5% (nine degrees of freedom) and the uncertainties in the derived order parameters do not exceed 20% of their values. It is worth noting that equation (5) does not explicitly take into account motions on the nanosecond time-scale. If these motions are present, values of the correlation times and order parameters depend on the actual dynamics parameters in complex ways.[54] In our study, however, we focus on identification of differences in barnase dynamics between free and barstar-bound forms, while avoiding quantitative interpretation in terms of specific dynamic models.

Overall tumbling

Rotational correlation times were calculated both from ratios of ^{15}N R_1 and R_2 values,[55] and from the model-free analysis of ^{2}H relaxation rates using data from all resolved peaks in the spectra. Corresponding apparent molecular correlation times τ_R were calculated as averages over

values for individual amides or methyl groups. A value of $<\tau_R^{eff}>=5.3(\pm0.8)$ ns, as averaged over all methyl groups, was obtained from the ^{2}H relaxation data on free barnase that matches the value obtained from the backbone ^{15}N relaxation measurements, 5.8(±0.02) ns. Although τ_R^{eff} values for each methyl group were not significantly higher than average, values for six methyl groups, A1β, V3γ1, I55δ1, I96δ1, T105γ2 and T107γ2, are below the average by more than one standard deviation. All these methyl groups are found on the protein surface and may undergo nanosecond motions. Excluding these six residues from the average give $<\tau_R^{eff}>=5.6(\pm0.4)$ ns, even closer to the value derived from the ^{15}N data.

Rotational correlation times calculated for the barnase–barstar complex from ^{15}N and ^{2}H data are also in good agreement, 12.5(±0.08) ns and 11.9(±1.4) ns, respectively. It should be noted, however, that while free barnase shows no signs of aggregation under the sample conditions used in our experiments, barstar tends to dimerize, and there is approximately 20% dimer formed at the millimolar protein concentrations used here.[56] Sites responsible for barstar dimerization and for the interaction with barnase do not overlap and one can anticipate that the barnase–barstar complex would also dimerize with a binding constant similar to that obtained for free barstar. Indeed, τ_R values of 10.7(±0.1) ns and 12.5(±0.08) ns were obtained from ^{15}N R_1 and R_2 measurements on dilute (0.17 mM) and concentrated samples of the complex, respectively. This indicates a concentration-dependent aggregation, which complicates the model-free analysis,[57] and increases errors in the dynamic parameters extracted from relaxation data for the complex. The concentration-dependent fraction of the barnase–barstar dimer, ν, was estimated using the equation:

$$\nu = (\tau_R - \tau_R^M)/(\tau_R^D - \tau_R^M) \quad (6)$$

where τ_R is the apparent rotational correlation time obtained from ^{15}N relaxation measurements, and τ_R^D and τ_R^M are theoretical estimates of the correlation times of dimer and monomer respectively. These values were calculated using the following equation (equation 42 of Daragan & Mayo[58]):

$$\tau_R^N = (9.18 \times 10^{-3}/T)\exp(2416/T)\,N^{0.93} \quad (7)$$

where N, the number of amino acid residues, equals 199 and 398 for the monomer and dimer barnase–barstar complexes, respectively, T is the temperature (in K) and all correlation times are in nanoseconds. In this way, the dimer concentration is estimated at 8(±8) % and 27(±8) % for concentrations of 0.17 mM and 1.17 mM (used in the experiments here), which is consistent with expectations based on the dimerization constant for free barstar.

In order to estimate possible errors in the analysis of methyl dynamics that are introduced by the partial dimerization of the complex, we have carried out additional simulations based on a formalism that includes exchange between monomer and dimer (e.g. see equations 5.134, 5.135 of Cavanagh *et al.*[59]). Synthetic ^{2}H relaxation rates were generated for exchange extending from fast to slow, for dimer fractions up to 27%, and for axial order parameters and internal correlation times systematically sampled in the ranges 0.1–1.0 and 10–100 ps, respectively. Overall rotational correlation times of 11 ns and 22 ns were assumed for the barnase–barstar complex and dimer of the complex, respectively. The extracted rates were subsequently fit in a manner analogous to the experimental data, and the highest systematic errors in S^2 and τ_e were 7% and 4%, respectively. In practice, we expect smaller errors, since magnetization from the dimer will decay more efficiently during the significant magnetization transfer steps in the experiments, effectively reducing the contribution of the dimer fraction to the measured relaxation rates. To account for these and other systematic errors in our analysis, we set lower bound on uncertainties for S^2 of 4% and 7%, and for τ_e of 3% and 4% for free barnase and its complex, respectively. Additionally, the methyl group of A11β was excluded from analysis due to its very high apparent τ_R value in the complex.

Differences in dynamics

Changes in dynamics upon ligand binding were identified using a statistical Z-score.[60] The Z-score is calculated as a ratio of the difference in dynamic parameters (S^2_{axis} or τ_e) and the corresponding experimental error, estimated as a geometric sum of the experimental errors for measurements on free barnase and the complex. We assume that a difference in dynamics is statistically significant for an individual methyl if at least one of the two Z-scores calculated for S^2_{axis} and τ_e exceeds 1.96, which corresponds to the 5% probability cut-off. No statistical correction was done to account for multiple comparisons for different methyl groups.

MD simulations of free barnase and of the barnase–barstar complex

Two MD runs of 30 ns each were performed on free barnase and the complex of barnase and barstar(C40,82A) in water. The parallel version of the Gromacs package,[61,62] the all-hydrogen force field OPLS-AA/L[63,64] and the TIP4P[65] water model were used for the simulations. The following crystal structures from the Protein Data Bank were taken as starting points: entry 1A2P (structure B) for the free barnase run and entry 1B27 (structures A and D) for the simulation of the barnase–barstar (C40,82A) complex. The initial structures with crystallographic water molecules were solvated in rhombic dodecahedrons such that the minimal thickness of the explicit water layer around the solute was 9 Å. This resulted in 5769 and 11003 water molecules in the systems containing free barnase and the complex, respectively. Charges of the protein amino acids were chosen to mimic an experimental pH value of 6.5. His102 of barnase and His17 of barstar were considered neutral. A positive charge was assigned to His18 of barnase, which had been shown to have an anomalously high pK_a.[66] In order to neutralize each of the protein systems, water molecules with the most favorable electrostatic potential were replaced by ions. Three Cl^- and three K^+ were required to compensate the positive charge of free barnase and the negative charge of the complex, respectively. The systems were equilibrated before and after insertion of ions. The equilibration protocol included an energy minimization followed by a 50 ps dynamics trajectory with harmonic position restraints on all protein heavy-atoms (force constant of 1000 kJ mol^{-1}nm^{-2}).

MD simulations of the systems were then performed under the following conditions: all bonds with hydrogen atoms were constrained by the LINCS algorithm,[67] allowing time-steps of 2 fs; temperature and pressure were controlled using Berendsen weak coupling[68] at 300 K and 1 bar with coupling times of 0.2 ps and 2 ps, respectively; a neighbor list for non-bonded interactions based on a cutoff of 9 Å was used and updated every five

steps; Coulomb interactions were computed with the PME method;[69,70] all simulations were run with periodic boundary conditions; atomic coordinates were stored for analysis every 0.5 ps. Intervals of 3–33 ns for the trajectory of free barnase and 1–31 ns for the trajectory of the complex were used for analysis. Overall molecular motions were removed by superimposing MD trace structures with the corresponding average structures. Only backbone atoms from rigid parts of barnase were used for superposition, i.e. from residues 5–36, 41–56, 69–76, and 85–110. All calculations were performed on a Linux cluster with 48 AMD Opteron 2.4 GHz processors and Infiniband communication.

Calculation of order parameters from MD trajectories

The whole MD trajectory was split into several time segments of the length $L = 500$ ps. Order parameters $S^2_{\mathrm{axis}}(L)$ were estimated from distributions of the directions of methyl rotation axes. The order parameters $S^2_{\mathrm{axis}}(L)$ were calculated using a slightly modified form of equation 3.17 from the review by Korzhnev *et al.*[47]:

$$S^2_{\mathrm{axis}}(L) = \left\langle \frac{1}{N^2} \sum_{i=1}^{N} \sum_{j=1}^{N} P_2\left(\mu_i \mu_j\right) \right\rangle_{\mathrm{segments}} \qquad (8)$$

where μ is a unit vector directed along the methyl ^{13}C-^{13}C axis, N is the number of snapshots in one segment, and the indexes i and j run over all snapshots in the segment. Angular brackets denote averaging over all segments in the MD trace. Uncertainties of the $S^2_{\mathrm{axis}}(L)$ values were estimated as the standard deviation of order parameters obtained independently with the above procedure for each of the six consecutive 5 ns fragments of the 30 ns MD trace. Although the MD order parameters are calculated using time segments of length $L = 500$ ps, the correlation coefficients between the experimental and MD order parameters do not change significantly when varying L from 100 ps to 1000 ps.

Dynamic domains

High-amplitude correlated motions of barnase were extracted from the MD traces using PCA with a mass weighted covariance matrix.[29] The two 30 ns MD traces for both free and bound barnase were divided into ten 3 ns segments each and the PCA was performed for individual segments. The covariance matrices for the segments were calculated and diagonalized using the Gromacs program.[62] N, C′, C^{α} and C^{β} atoms for residues 5–110 of barnase were used when computing the covariance matrices; the first four N-terminal residues were excluded because of their high flexibility. Before the analysis, overall rotations and translations were filtered out from the individual MD segments by superimposing the snapshots with the last structure of the corresponding segment using backbone atoms (N, C′ and C^{α}) from residues 5–36, 41–56, 69–76, and 85–110 (i.e. excluding flexible parts). In further analyses, we used the three PCA modes with the largest eigenvalues obtained for each of the 10×2 segments.

Dynamic domains were identified using an approach described previously,[30,31] and implemented in the DynDom software (version 1.50). The method allows one to represent the transition between two different protein structures as rotations and translations involving only a few rigid modules. As input, it accepts two protein spatial structures (since N, C′, C^{α} and C^{β} atoms are needed, pseudo-C^{β} positions are assumed for glycine residue). A pair of the most different structures was selected from the MD trajectory segment, which was modified so that only motions along a particular PCA mode are present. On output, DynDom produced rotation vectors for small segments (five residues) centered at individual residues. These vectors describe the transformation necessary to superimpose a given fragment from the first structure to the same fragment in the second structure. Positive and negative inner products of these vectors for different residues indicate approximately parallel and anti-parallel motions of these residues relative to each other. The inner products for all pairs of vectors define a symmetric rotation-orientation matrix. Visual analysis of 30×2 matrices (ten MD segments, three PCA modes for free and barstar-bound barnase) reveals five rigid modules: M1, residues 6–23; M2, residues 25–51; M3, residues 54–74; M4, residues 75–87; and M5, residues 90–107, and bending regions between them in the protein amino acid sequence (Figure 3). The modules are seen in Figure 7, which shows two rotation-orientation matrices (depicted above and below the diagonal) for barnase in the free and bound forms (see also Figure 3). The matrices were calculated as averages over matrices obtained for individual the MD segments and PCA modes. The modules can be grouped into dynamic domains based on their relative motions. For example, rotation vectors from the modules M1 and M2 show clear anti-correlation (Figure 7), which proves that these modules belong to different dynamic domains.

Characterization of collective motions using the GNM approach

Collective motions over a wide range of time-scales spanning beyond the limits accessible for MD simulations were characterized using an extension of the GNM. The model is described in more detail elsewhere,[32,33] and is

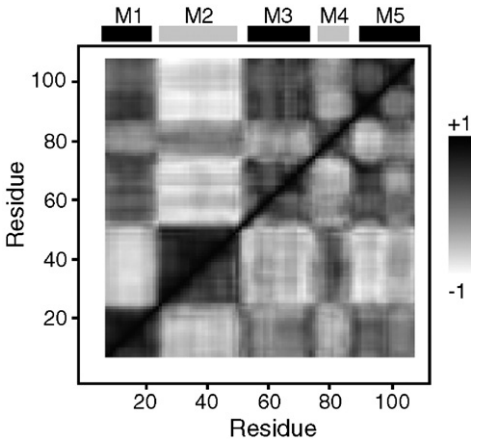

Figure 7. Two average rotation–orientation matrices (depicted above and below the diagonal) for barnase in the free and bound forms. The matrices were calculated as averages of those obtained for individual MD segments and PCA modes (see the text for details). Positive (black) and negative (white) values are associated with approximately parallel and anti-parallel motions of the two residues, respectively. Five rigid modules (M1–M5, see the text) separated by four bending regions are shown above the plot.

implemented in the GNM_V1.3.1 software.† In short, an elastic network was built using positions of C^{α} atoms, which the software extracted from the PDB structure of free barnase (PDB code 1A2P). The normal mode analysis was performed using harmonic potentials with a single force constant accounting for pair-wise interactions between all C^{α} atoms within a 7 Å distance cut-off. The Debye-Waller factors (*B*-factors) predicted in our GNM analysis correlate well with the values found in the barnase crystal structure (correlation coefficient is 0.72), providing confidence in the computation. Bending regions between relatively rigid modules (Figure 3) were obtained using two GNM eigenvectors corresponding to the lowest frequencies as described in reference.[71] Similar locations of the bending regions were obtained for other barnase structures; namely, barnase in the complex with barstar (code 1BGS) and the set of 20 NMR structures (1BNR).

Data base codes

The experimental data for free and barstar-bound barnase are deposited together with parameters of fast methyl dynamics in the BMRB database (deposition codes 7139 and 7126, respectively).

Acknowledgements

This work was supported by research grants from the Swedish Research Council (621-2003-3095, 621-2003-4048, 621-2005-2951), RFBR (05-04-49342), the Russian Federal Agency for Science and Innovations, and the Russian Academy of Sciences (the program Molecular and Cell Biology). D.M.K. acknowledges a post-doctoral fellowship from the Canadian Institutes of Health Research Training Program in Protein Folding and Disease. L.E.K. holds a Canada Research Chair in Biochemistry.

References

1. Gunasekaran, K., Ma, B. Y. & Nussinov, R. (2004). Is allostery an intrinsic property of all dynamic proteins? *Proteins: Struct. Funct. Genet.* 57, 433–443.
2. Monod, J., Wyman, J. & Changeux, J. P. (1965). On the nature of allosteric transitions - a plausible model. *J. Mol. Biol.* 12, 88–118.
3. Koshland, D. E., Nemethy, G. & Filmer, D. (1966). Comparison of experimental binding data and theoretical models in proteins containing subunits. *Biochemistry*, 5, 365–385.
4. Weber, G. (1972). Ligand binding and internal equilibria in proteins. *Biochemistry*, 11, 864–878.
5. Kumar, S., Ma, B. Y., Tsai, C. J., Sinha, N. & Nussinov, R. (2000). Folding and binding cascades: dynamic landscapes and population shifts. *Protein Sci.* 9, 10–19.
6. Swain, J. F. & Gierasch, L. M. (2006). The changing landscape of protein allostery. *Curr. Opin. Struct. Biol.* 16, 102–108.
7. Hilser, V. J. & Freire, E. (1996). Structure-based calculation of the equilibrium folding pathway of proteins. Correlation with hydrogen exchange protection factors. *J. Mol. Biol.* 262, 756–772.
8. Ma, B. Y., Kumar, S., Tsai, C. J. & Nussinov, R. (1999). Folding funnels and binding mechanisms. *Protein Eng.* 12, 713–720.
9. Cooper, A. & Dryden, D. T. F. (1984). Allostery without conformational change - a plausible model. *Eur. Biophys. J. Biophys. Letters*, 11, 103–109.
10. Frauenfelder, H., Sligar, S. G. & Wolynes, P. G. (1991). The energy landscapes and motions of proteins. *Science*, 254, 1598–1603.
11. Popovych, N., Sun, S. J., Ebright, R. H. & Kalodimos, C. G. (2006). Dynamically driven protein allostery. *Nature Struct. Mol. Biol.* 13, 831–838.
12. Fuentes, E. J., Der, C. J. & Lee, A. L. (2004). Ligand-dependent dynamics and intramolecular signaling in a PDZ domain. *J. Mol. Biol.* 335, 1105–1115.
13. Millet, O., Mittermaier, A., Baker, D. & Kay, L. E. (2003). The effects of mutations on motions of side-chains in protein L studied by H-2 NMR dynamics and scalar couplings. *J. Mol. Biol.* 329, 551–563.
14. Zhang, Y. B. & Zuiderweg, E. R. P. (2004). The 70-kDa heat shock protein chaperone nucleotide-binding domain in solution unveiled as a molecular machine that can reorient its functional subdomains. *Proc. Natl Acad. Sci. USA*, 101, 10272–10277.
15. Revington, M., Zhang, Y. B., Yip, G. N. B., Kurochkin, A. V. & Zuiderweg, E. R. P. (2005). NMR investigations of allosteric processes in a two-domain Thermus thermophilus Hsp70 molecular chaperone. *J. Mol. Biol.* 349, 163–183.
16. Revington, M., Holder, T. M. & Zuiderweg, E. R. P. (2004). NMR study of nucleotide-induced changes in the nucleotide binding domain of *Thermus thermophilus* Hsp70 chaperone DnaK - implications for the allosteric mechanism. *J. Biol. Chem.* 279, 33958–33967.
17. Buckle, A. M., Schreiber, G. & Fersht, A. R. (1994). Protein-protein recognition - crystal structural-analysis of a barnase barstar complex at 2.0-angstrom resolution. *Biochemistry*, 33, 8878–8889.
18. Hilser, V. J., Dowdy, D., Oas, T. G. & Freire, E. (1998). The structural distribution of cooperative interactions in proteins: analysis of the native state ensemble. *Proc. Natl Acad. Sci. USA*, 95, 9903–9908.
19. Serrano, L., Kellis, J. T., Cann, P., Matouschek, A. & Fersht, A. R. (1992). The folding of an enzyme .2. Substructure of barnase and the contribution of different interactions to protein stability. *J. Mol. Biol.* 224, 783–804.
20. Nolde, S. B., Arseniev, A. S., Orekhov, V. Y. & Billeter, M. (2002). Essential domain motions in barnase revealed by MD simulations. *Proteins: Struct. Funct. Genet.* 46, 250–258.
21. Giraldo, J., De Maria, L. & Wodak, S. J. (2004). Shift in nucleotide conformational equilibrium contributes to increased rate of catalysis of GpAp versus GpA in barnase. *Proteins: Struct. Funct. Bioinf.* 56, 261–276.
22. Millet, O., Muhandiram, D. R., Skrynnikov, N. R. & Kay, L. E. (2002). Deuterium spin probes of side-chain dynamics in proteins. 1. Measurement of five relaxation rates per deuteron in C-13-labeled and fractionally H-2-enriched proteins in solution. *J. Am. Chem. Soc.* 124, 6439–6448.
23. Lipari, G. & Szabo, A. (1982). Model-free approach to the interpretation of nuclear magnetic-resonance relaxation in macromolecules. 1. Theory and range of validity. *J. Am. Chem. Soc.* 104, 4546–4559.

† ignm.ccbb.pitt.edu

24. Lipari, G. & Szabo, A. (1982). Model-free approach to the interpretation of nuclear magnetic-resonance relaxation in macromolecules. 2. Analysis of experimental results. *J. Am. Chem. Soc.* 104, 4559–4570.
25. Best, R. B., Clarke, J. & Karplus, M. (2004). The origin of protein sidechain order parameter distributions. *J. Am. Chem. Soc.* 126, 7734–7735.
26. Mittermaier, A., Kay, L. E. & Forman-Kay, J. D. (1999). Analysis of deuterium relaxation-derived methyl axis order parameters and correlation with local structure. *J. Biomol. NMR*, 13, 181–185.
27. Ming, D. M. & Bruschweiler, R. (2004). Prediction of methyl-side chain dynamics in proteins. *J. Biomol. NMR*, 29, 363–368.
28. Best, R. B., Clarke, J. & Karplus, M. (2005). What contributions to protein side-chain dynamics are probed by NMR experiments? A molecular dynamics simulation analysis. *J. Mol. Biol.* 349, 185–203.
29. Kitao, A. & Go, N. (1999). Investigating protein dynamics in collective coordinate space. *Curr. Opin. Struct. Biol.* 9, 164–169.
30. Hayward, S., Kitao, A. & Berendsen, H. J. C. (1997). Model-free methods of analyzing domain motions in proteins from simulation: a comparison of normal mode analysis and molecular dynamics simulation of lysozyme. *Proteins: Struct. Funct. Genet.* 27, 425–437.
31. Hayward, S. & Berendsen, H. J. C. (1998). Systematic analysis of domain motions in proteins from conformational change: new results on citrate synthase and T4 lysozyme. *Proteins: Struct. Funct. Genet.* 30, 144–154.
32. Bahar, I., Atilgan, A. R. & Erman, B. (1997). Direct evaluation of thermal fluctuations in proteins using a single-parameter harmonic potential. *Fold. Des.* 2, 173–181.
33. Haliloglu, T., Bahar, I. & Erman, B. (1997). Gaussian dynamics of folded proteins. *Phys. Rev. Letters*, 79, 3090–3093.
34. Yanagawa, H., Yoshida, K., Torigoe, C., Park, J. S., Sato, K., Shirai, T. & Go, M. (1993). Protein anatomy - functional roles of barnase module. *J. Biol. Chem.* 268, 5861–5865.
35. Salvatella, X., Dobson, C. M., Fersht, A. R. & Vendruscolo, M. (2005). Determination of the folding transition states of barnase by using Phi(I)-value-restrained simulations validated by double mutant Phi(IJ)-values. *Proc. Natl Acad. Sci. USA*, 102, 12389–12394.
36. Rousseau, F. & Schymkowitz, J. (2005). A systems biology perspective on protein structural dynamics and signal transduction. *Curr. Opin. Struct. Biol.* 15, 23–30.
37. Chatfield, D. C., Augsten, A. & D'Cunha, C. (2004). Correlation times and adiabatic barriers for methyl rotation in SNase. *J. Biomol. NMR*, 29, 377–385.
38. Formaneck, M. S., Ma, L. & Cui, Q. (2006). Reconciling the "old" and "new" views of protein allostery: a molecular simulation study of chemotaxis Y protein (Che Y). *Proteins: Struct. Funct. Genet.* 63, 846–867.
39. Axe, D. D., Foster, N. W. & Fersht, A. R. (1998). A search for single substitutions that eliminate enzymatic function in a bacterial ribonuclease. *Biochemistry*, 37, 7157–7166.
40. Axe, D. D., Foster, N. W. & Fersht, A. R. (1999). An irregular beta-bulge common to a group of bacterial RNases is an important determinant of stability and function in barnase. *J. Mol. Biol.* 286, 1471–1485.
41. Clarkson, M. W. & Lee, A. L. (2004). Long-range dynamic effects of point mutations propagate through side chains in the serine protease inhibitor eglin c. *Biochemistry*, 43, 12448–12458.
42. Clarkson, M. W., Gilmore, S. A., Edgell, M. H. & Lee, A. L. (2006). Dynamic coupling and allosteric behavior in a nonallosteric protein. *Biochemistry*, 45, 7693–7699.
43. Lockless, S. W. & Ranganathan, R. (1999). Evolutionarily conserved pathways of energetic connectivity in protein families. *Science*, 286, 295–299.
44. Suel, G. M., Lockless, S. W., Wall, M. A. & Ranganathan, R. (2003). Evolutionarily conserved networks of residues mediate allosteric communication in proteins. *Nature Struct. Biol.* 10, 59–69.
45. Korzhnev, D. M., Bocharov, E. V., Zhuravlyova, A. V., Tischenko, E. V., Reibarkh, M. Y., Ermolyuk, Y. S. *et al.* (2001). H-1, C-13 and N-15 resonance assignment for barnase. *Appl. Magn. Reson.* 21, 195–201.
46. Bartels, C., Xia, T. H., Billeter, M., Guntert, P. & Wuthrich, K. (1995). The program Xeasy for computer-supported NMR spectral analysis of biological macromolecules. *J. Biomol. NMR*, 6, 1–10.
47. Korzhnev, D. M., Billeter, M., Arseniev, A. S. & Orekhov, V. Y. (2001). NMR studies of Brownian tumbling and internal motions in proteins. *Prog. Nucl. Magn. Reson. Spectrosc.* 38, 197–266.
48. Delaglio, F., Grzesiek, S., Vuister, G. W., Zhu, G., Pfeifer, J. & Bax, A. (1995). NMRPipe - a multidimensional spectral processing system based on Unix Pipes. *J. Biomol. NMR*, 6, 277–293.
49. Korzhnev, D. M., Ibraghimov, I. V., Billeter, M. & Orekhov, V. Y. (2001). MUNIN: application of three-way decomposition to the analysis of heteronuclear NMR relaxation data. *J. Biomol. NMR*, 21, 263–268.
50. Orekhov, V. Y., Nolde, D. E., Golovanov, A. P., Korzhnev, D. M. & Arseniev, A. S. (1995). Processing of heteronuclear NMR relaxation data with the new software DASHA. *Appl. Magn. Reson.* 9, 581–588.
51. Zhuravleva, A. V., Korzhnev, D. M., Kupce, E., Arseniev, A. S., Billeter, M. & Orekhov, V. Y. (2004). Gated electron transfers and electron pathways in azurin: a NMR dynamic study at multiple fields and temperatures. *J. Mol. Biol.* 342, 1599–1611.
52. Farrow, N. A., Muhandiram, R., Singer, A. U., Pascal, S. M., Kay, C. M., Gish, G. *et al.* (1994). Backbone dynamics of a free and a phosphopeptide-complexed Src homology-2 domain studied by N-15 NMR relaxation. *Biochemistry*, 33, 5984–6003.
53. Skrynnikov, N. R., Millet, O. & Kay, L. E. (2002). Deuterium spin probes of side-chain dynamics in proteins. 2. Spectral density mapping and identification of nanosecond time-scale side-chain motions. *J. Am. Chem. Soc.* 124, 6449–6460.
54. W.Y. Choy, L.E. Kay, Model selection for the interpretation of protein side chain methyl dynamics. *J. Biomol. NMR*, 25 (2003) 325–333.
55. Tjandra, N., Feller, S. E., Pastor, R. W. & Bax, A. (1995). Rotational diffusion anisotropy of human ubiquitin from N-15 NMR relaxation. *J. Am. Chem. Soc.* 117, 12562–12566.
56. Korchuganov, D. S., Nolde, S. B., Reibarkh, M. Y., Orekhov, V. Y., Schulga, A. A., Ermolyuk, Y. S. *et al.* (2001). NMR study of Monomer-dimer equilibrium of barstar in solution. *J. Am. Chem. Soc.* 123, 2068–2069.
57. Schurr, J. M., Babcock, H. P. & Fujimoto, B. S. (1994). A Test of the model-free formulas - effects of anisotropic rotational diffusion and dimerization. *J. Magn. Reson. ser. B*, 105, 211–224.
58. Daragan, V. A. & Mayo, K. H. (1997). Motional model analyses of protein and peptide dynamics using C-13

and N-15 NMR relaxation. *Prog. Nucl. Magn. Reson. Spectrosc.* 31, 63–105.
59. Cavanagh, J., Fairbrother, W., Palmer, A. & Skelton, N. (1995). *Protein NMR Spectroscopy: Principles and Practice.* Academic Press, San Diego.
60. Mittermaier, A. & Kay, L. E. (2004). The response of internal dynamics to hydrophobic core mutations in the SH3 domain from the Fyn tyrosine kinase. *Protein Sci.* 13, 1088–1099.
61. Lindahl, E., Hess, B. & van der Spoel, D. (2001). GROMACS 3.0: a package for molecular simulation and trajectory analysis. *J. Mol. Model.* 7, 306–317.
62. Berendsen, H. J. C., Vanderspoel, D. & Vandrunen, R. (1995). Gromacs - a message-passing parallel molecular-dynamics implementation. *Comput. Phys. Commun.* 91, 43–56.
63. Jorgensen, W. L. & Tiradorives, J. (1988). The Opls potential functions for proteins - energy minimizations for crystals of cyclic-peptides and crambin. *J. Am. Chem. Soc.* 110, 1657–1666.
64. Kaminski, G. A., Friesner, R. A., Tirado-Rives, J. & Jorgensen, W. L. (2001). Evaluation and reparametrization of the OPLS-AA force field for proteins via comparison with accurate quantum chemical calculations on peptides. *J. Phys. Chem. B*, 105, 6474–6487.
65. Jorgensen, W. L., Chandrasekhar, J., Madura, J. D., Impey, R. W. & Klein, M. L. (1983). Comparison of simple potential functions for simulating liquid water. *J. Chem. Phys.* 79, 926–935.
66. Loewenthal, R., Sancho, J. & Fersht, A. R. (1992). Histidine aromatic interactions in barnase - elevation of histidine pK_a and contribution to protein stability. *J. Mol. Biol.* 224, 759–770.
67. Hess, B., Bekker, H., Berendsen, H. J. C. & Fraaije, J. (1997). LINCS: a linear constraint solver for molecular simulations. *J. Comput. Chem.* 18, 1463–1472.
68. Berendsen, H. J. C., Postma, J. P. M., Vangunsteren, W. F., Dinola, A. & Haak, J. R. (1984). Molecular-dynamics with coupling to an external bath. *J. Chem. Phys.* 81, 3684–3690.
69. Darden, T., York, D. & Pedersen, L. (1993). Particle mesh Ewald - an N.Log(N) method for Ewald sums in large systems. *J. Chem. Phys.* 98, 10089–10092.
70. Essmann, U., Perera, L., Berkowitz, M. L., Darden, T., Lee, H. & Pedersen, L. G. (1995). A smooth particle mesh Ewald method. *J. Chem. Phys.* 103, 8577–8593.
71. Yang, L. W., Liu, X., Jursa, C. J., Holliman, M., Rader, A., Karimi, H. A. & Bahar, I. (2005). iGNM: a database of protein functional motions based on a Gaussian network model. *Bioinformatics*, 21, 2978–2987.

Edited by A. G. Palmer

(Received 1 December 2006; received in revised form 9 January 2007; accepted 19 January 2007)
Available online 24 January 2007